

# A gene signal amplifier platform for monitoring the unfolded protein response

Carlos A. Origel Marmolejo <sup>1</sup>, Bhagyashree Bachhav <sup>2</sup>, Sahiti D. Patibandla Alexander L. Yang and Laura Segatori <sup>1</sup>, Alexander L. Yang and Laura Segator

Gene expression in mammalian cells results from coordinated protein-driven processes guided by diverse mechanisms of regulation, including protein-protein interactions, protein localization, DNA modifications and chromatin rearrangement. Regulation of gene expression is particularly important in stress-response pathways. To address the need to monitor chromosomal gene expression generating a readily detectable signal output that recapitulates gene expression dynamics, we developed a gene signal amplifier platform that links transcriptional and post-translational regulation of a fluorescent output to the expression of a chromosomal target gene. We generated a multiplex reporter system for monitoring markers of the unfolded protein response, a complex signal transduction pathway that remodels gene expression in response to proteotoxic stress in the endoplasmic reticulum. By recapitulating the transcriptional and translational control mechanisms underlying the expression of a target gene with high sensitivity, this platform provides a technology for monitoring gene expression with superior sensitivity and dynamic resolution.

he complex set of instructions stored in the genome of mammalian cells is precisely translated through highly integrated regulatory processes that control gene expression spatially and temporally. Stress-response signaling pathways rely on coordinated regulation of gene expression to restore cellular homeostasis in response to intracellular and environmental stimuli¹. Not surprisingly, abnormal expression levels of genes mediating stress-responses have been linked to the development of a range of diseases, including Alzheimer's disease², diabetes³ and several types of cancer⁴. Accurate detection of gene expression signatures associated with pathogenicity⁵ is thus expected to inform the design of effective treatment strategies for a variety of diseases.

Gene expression is mostly measured using tools for quantifying gene transcription, including DNA microarrays6 and quantitative PCR with reverse transcription (RT-qPCR)7, which are ideally suited to produce snapshots of the cell transcriptome8. These technologies, however, do not provide temporal resolution of gene expression dynamics. Reporter gene assays based on minimal or synthetic regulatory sequences enable facile detection of gene expression, but often fail to recapitulate the native chromosomal context of the target gene involving multiple layers of control and trans-acting enhancers9, and are often plagued by signal variability and instability. Here we report a versatile gene signal amplifier platform technology for monitoring gene expression designed to profile endogenous regulatory mechanisms with high sensitivity and resolution of gene dynamics. The expression of a fluorescent reporter was linked to that of an endogenous target through a tunable orthogonal gene network and post-translational control elements specially designed to amplify the signal output for accurate detection of the transcriptional and translational regulatory mechanisms that control expression of the target gene. The platform was implemented through chromosomal integration of the main control element using CRISPR-Cas9 (clustered, regularly interspaced, short palindromic repeat-CRISPR-associated protein 9)10 to link the genetic circuit to a target gene, thereby easily adapting the system to monitor any cellular target.

We demonstrated the use of the gene signal amplifier platform technology to quantify the unfolded protein response (UPR), a complex series of signaling cascades activated in response to proteotoxic stress in the endoplasmic reticulum (ER). The UPR manifests through activation of three interconnected signaling pathways controlling a transcriptional and translational regulatory program aimed at relieving ER stress through ER enlargement, upregulation of protein quality control components and inhibition of general protein translation to decrease ER protein load. These integrated signal transduction pathways are mediated by three ER membrane proteins that function as stress sensors: inositol-requiring kinase 1 (IRE1), dsRNA-induced protein kinase-like ER kinase (PERK) and activating transcription factor 6 (ATF6)11. Proteotoxic stress results in activation of these ER sensors and upregulation of partially overlapping sets of genes involved in protein quality control, ER-associated degradation components and lipid biosynthesis<sup>11</sup>. After sustained ER stress, however, the UPR executes apoptosis, pointing to underlying regulatory mechanisms that integrate information about the nature of the stress stimuli and shape the relative activation kinetics of the three signaling responses, ultimately dictating cell fate<sup>12,13</sup>. Specifically, IRE1 mediates splicing of the X-box binding protein (XBP1) messenger RNA, increasing the levels of spliced XBP1, which controls expression of genes involved in protein folding, ER-associated degradation, ER expansion and, eventually, apoptosis11 (Fig. 1a). Activated PERK mediates phosphorylation of eukaryotic translation initiator factor  $2\alpha$  (eIF2 $\alpha$ ), causing inhibition of general protein translation and selective translation of ATF4, which initially activates expression of pro-survival genes involved in protein folding, resistance to oxidative stress and autophagy, and, at later stages of ER stress, apoptosis<sup>14</sup> (Fig. 1a). ER stress also results in translocation of ATF6 to the Golgi and release of an activated form of ATF6 that controls expression of ER quality control proteins<sup>15</sup> (Fig. 1a).

<sup>1</sup>BioScience Department, Rice University, Houston, TX, USA. <sup>2</sup>Chemical and Biomolecular Engineering Department, Rice University, Houston, TX, USA. <sup>3</sup>Department of Computational and Applied Mathematics, Rice University, Houston, TX, USA. <sup>4</sup>Bioengineering Department, Rice University, Houston, TX, USA. <sup>™</sup>e-mail: segatori@rice.edu

**ARTICLES** 

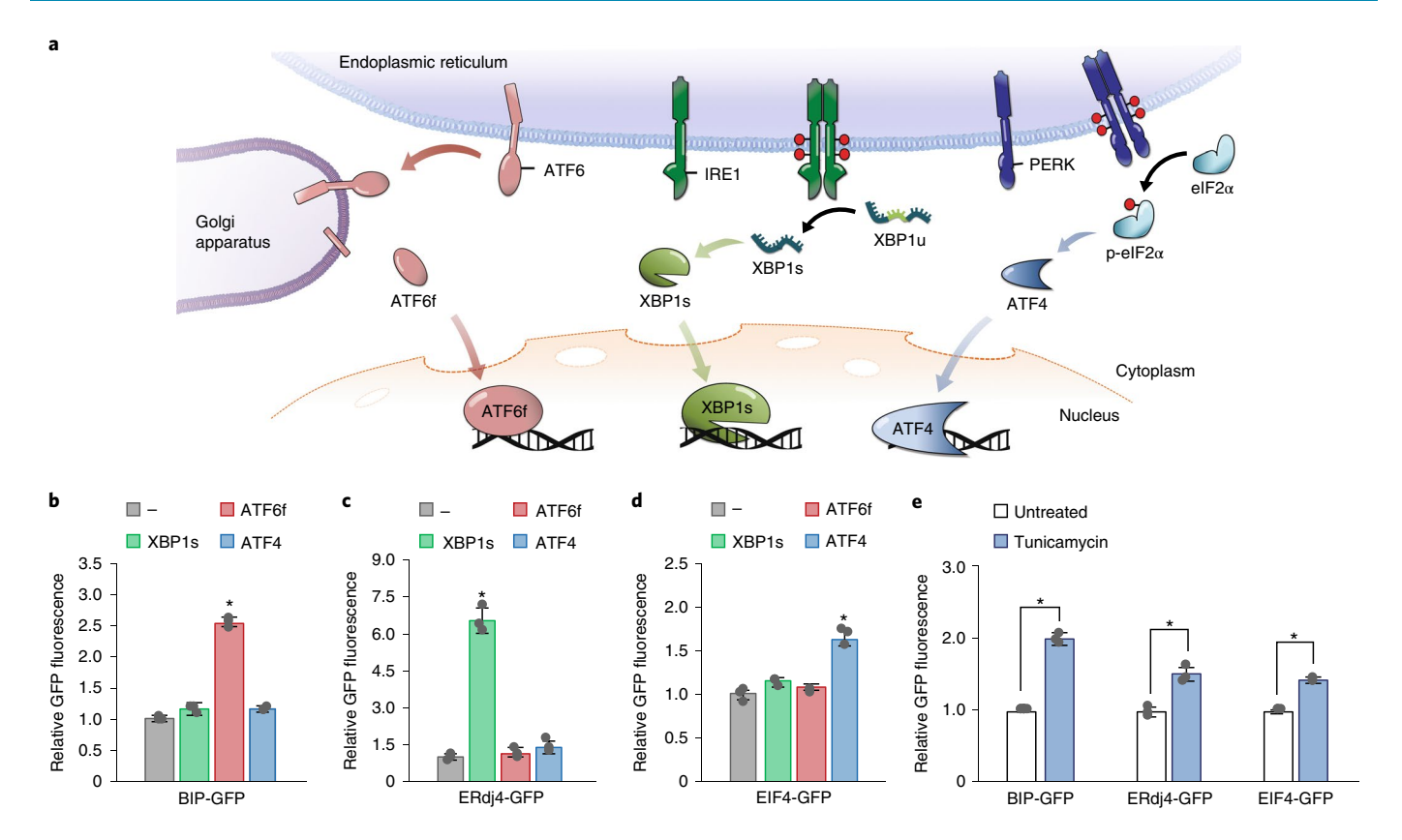


Fig. 1 | Monitoring UPR signaling pathway-specific target genes through chromosomal integration of a reporter gene. a, Schematic representation of the UPR. The three ER membrane sensors IRE1, PERK and ATF6 mediate activation of signal transduction pathways that results in upregulation of genes involved in stress attenuation and apoptosis. The red circle represents phosphorylation.  $\mathbf{b}$ - $\mathbf{d}$ , Flow cytometry analyses of BIP-GFP ( $\mathbf{b}$ ), ERdj4-GFP ( $\mathbf{c}$ ) and EIF4-GFP ( $\mathbf{d}$ ) cells transfected for the expression of XBP1s, ATF6f and ATF4. Relative GFP fluorescence values were obtained by normalizing the GFP fluorescence values of transfected cells to that of cells transfected with an empty vector (-). Data are reported as mean  $\pm$  s.d. (n=3,  $^*P$ <0.005).  $\mathbf{e}$ , Flow cytometry analyses of BIP-GFP, ERdj4-GFP and EIF4-GFP cells treated with tunicamycin (1 $\mu$ g ml<sup>-1</sup>, 24 h). Relative GFP fluorescence values were obtained by normalizing the GFP fluorescence values of treated cells to that of untreated cells. Data are reported as mean  $\pm$  s.d. (n=3,  $^*P$ <0.005).

The gene signal amplifier platform was validated by developing a multiplex reporter system for monitoring UPR markers of the three signaling pathways. A predictive mathematical model was also generated that allows adapting the gene signal amplifier for optimal detection of the expression of any cellular gene. By recapitulating the transcriptional and translational control mechanisms underlying expression of a target gene with high sensitivity, this platform provides an innovative technology for multiplex detection of mammalian gene expression that will enable characterization of gene expression signatures of physiologic and pathogenic processes.

#### Results

Chromosomal integration of the reporter for monitoring UPR genes. To generate a reporter system for profiling the expression of UPR genes that recapitulates the complexity of mammalian regulatory mechanisms involving chromatin rearrangement <sup>16</sup>, transcriptional cofactors <sup>17</sup> and trans-acting enhancers <sup>18</sup>, we placed the reporter under the same transcriptional and translational regulation as the UPR target gene. We developed a set of reporter cell lines in which the expression of the reporter is linked to that of a UPR target gene specifically upregulated upon activation of one UPR signaling pathway. We identified three genes expected to be regulated by one of the UPR-activated transcription factors and not to respond to cross-activation, namely *DNAJB9* (*ERdj4*) controlled by XBP1 (ref. <sup>12</sup>), *EIF4EBP1* (*EIF4*) controlled by ATF4 (ref. <sup>19</sup>) and *HSPA5* (*BIP*) controlled by ATF6 (ref. <sup>20</sup>). The chromosome of HEK293 cells was edited to integrate a cassette containing an internal ribosome

entry site (IRES) and the *GFP* gene (*IRES\_GFP*) downstream of *BIP*, *ERdj4* or *EIF4* using CRISPR–Cas9 via homologous direct-repair<sup>10</sup>. Chromosomal integration of *IRES\_GFP* results in transcription of a polycistronic mRNA encoding the target gene and *GFP*. We used the IRES from encephalomyocarditis virus<sup>21</sup> that does not affect the expression of the gene upstream of the *IRES* sequence<sup>22</sup> (Supplementary Fig. 1a) and is expected to lead to expression of the proteins encoded from the genes upstream and downstream of the IRES in a 1:3 ratio (Supplementary Fig. 1b). The integration cassette included the neomycin resistance gene expressed under a constitutive promoter, enabling selection of the cell lines BIP-GFP, ERdj4-GFP and EIF4-GFP (Supplementary Fig. 2).

To validate BIP-GFP, ERdj4-GFP and EIF4-GFP cell lines as reporters of the three UPR signaling pathways, cells were transiently transfected for the expression of the active forms of the UPR transcription factors, namely the spliced form of XBP1 (XBP1s) (ref. <sup>23</sup>), the cytosolic domain fragment of ATF6 (ATF6f) (ref. <sup>24</sup>) and the transcription factor ATF4 (ref. <sup>25</sup>). Flow cytometry measurements revealed an increase in GFP signal in each cell line only upon overexpression of the pathway-specific transcription factor (Fig. 1b–d), consistent with previously reported *BIP*, *ERdj4* and *EIF4* expression measurements<sup>12,19,26</sup>. These results indicate that linking the expression of a fluorescent reporter to that of *BIP*, *ERdj4* and *EIF4* generates UPR pathway-specific reporters.

To further characterize the reporter cell lines, we induced ER stress chemically using the canonical UPR inducers  $^{19,20}$ , namely tunicamycin ( $1 \mu g \, ml^{-1}$ ,  $24 \, h$ ), which affects glycoprotein processing  $^{27}$ , and

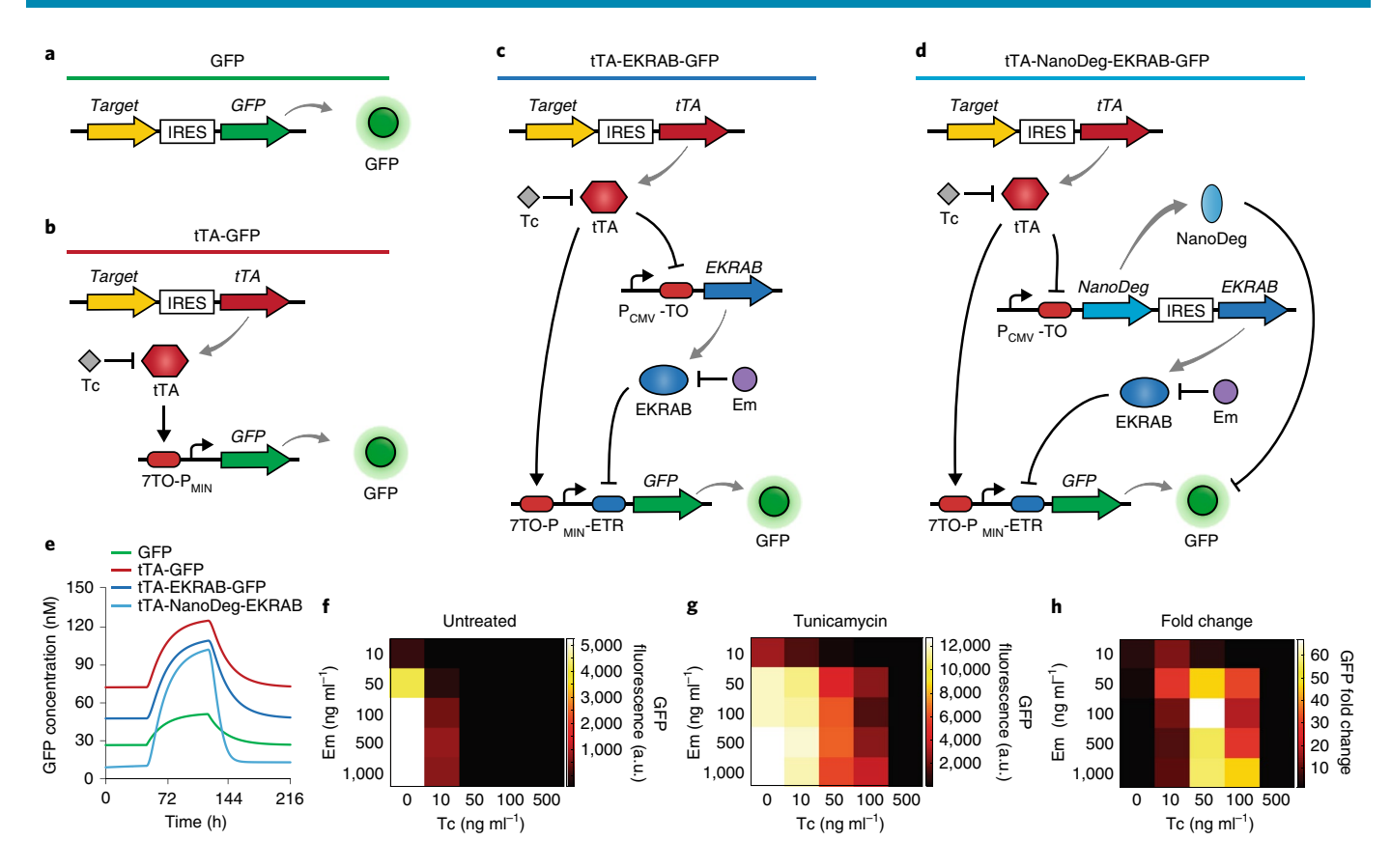


**Fig. 2** | **Design and implementation of the gene signal amplifier platform. a-d**, Schematic representation of genetic circuits topologies involving chromosomal integration of *IRES-GFP* (**a**) or chromosomal integration of *IRES-tTA* regulating activation of GFP (**b**), activation of GFP and repression of EKRAB that represses GFP (**c**) or activation of GFP and repression of EKRAB and the NanoDeg that represses and depletes GFP, respectively (**d**). **e**, Simulation of GFP expression from circuit topologies in **a-d** in response to a transient stimulus (from 48 h to 120 h) that induces a twofold change in the target gene expression. **f**,**g**, Flow cytometry analyses of MCL/BIP-tTA cells as a function of Tc and Em concentration reported as GFP fluorescence measurements under basal conditions (**f**) and upon treatment with tunicamycin (**g**) ( $1 \mu g ml^{-1}$ , 48 h). Data are reported as mean (n = 3). a.u., arbitrary units. **h**, Fold change of GFP fluorescence obtained by normalizing the GFP fluorescence measurements of MCL/BIP-tTA cells treated with tunicamycin (**g**) to that of untreated cells (**f**). Data are reported as mean (n = 3).

thapsigargin (1  $\mu$ M, 24h), which causes ER calcium depletion<sup>28</sup>, and observed an increase in GFP signal in BIP-GFP, ERdj4-GFP and EIF4-GFP cells (Fig. 1e and Supplementary Fig. 3), consistent with published results<sup>12,23</sup>.

Measurements of BIP protein levels in BIP-GFP cells (as representative of the three cell lines) and in the parental HEK293 cells confirmed that chromosomal integration of the reporter gene does not affect the expression of the UPR target gene (Supplementary Fig. 4).

Design of a gene signal amplifier platform. To improve the performance of the gene detection system with respect to signal amplification and dynamic resolution, we explored orthogonal regulatory elements for enhancing transcriptional and post-translational control of the reporter. Transcriptional control affects the reporter output sensitivity, while post-translational control improves the dynamic properties of the system, which are otherwise likely determined by the intrinsic stability of the reporter protein. We explored a series of circuit topologies that link expression of GFP to that of the target gene with the ultimate goal of developing a gene signal amplifier that recapitulates endogenous transcriptional regulatory mechanisms (Fig. 2). We built a deterministic mathematical model that simulates protein expression as dependent on the rate of protein production and degradation and on dilution due to cell growth (Supplementary Note). The output dynamic range of the

reporter based on chromosomal integration of GFP (Fig. 2a) was improved dramatically through extrachromosomal expression of GFP and chromosomal integration of an activator (the tetracyclinedependent transactivator, tTA)29 of GFP (Fig. 2b,e, compare green with red). Introducing a repressor (the erythromycin-dependent transrepressor, EKRAB)30 under negative control of tTA and placing GFP under control of a hybrid promoter that is activated by tTA and repressed by EKRAB lowers the output expression corresponding to basal expression of the target gene (Fig. 2c,e, blue). Introducing post-translational control of GFP by adding a GFP-specific NanoDeg31 under negative control of tTA further lowers GFP basal expression and accelerates GFP decay, thereby enhancing the output dynamic range and resolution of the input dynamics (Fig. 2d,e, cyan). The NanoDeg consists of a GFP-specific nanobody fused to a degradation tag (the 37-amino-acid carboxy-terminal sequence of ornithine decarboxylase) that mediates GFP degradation<sup>31</sup>. Optimal dynamic range of the GFP output and dynamic resolution of the target gene expression were thus achieved (1) by linking expression of a main regulator (tTA) to that of the target gene; and (2) by placing GFP under both positive transcriptional regulation (tTA), which mediates target signal amplification, and negative transcriptional (EKRAB) and post-translational (NanoDeg) regulation, which mediate GFP repression and decay, respectively (Fig. 2e).

We envisioned a master cell line harboring the circuit's components (that is, EKRAB, NanoDeg, GFP) that could be used to

generate gene-specific reporter cell lines through chromosomal integration of tTA downstream of a selected gene. The master cell line contains (1) GFP under the control of a hybrid promoter comprising a TTO operator for tTA activation and an ETR operator for EKRAB repression (7TO\_P<sub>MIN</sub>\_ETR\_GFP); and (2) the genes encoding NanoDeg and EKRAB linked through an IRES, under the control of the TO operator for tTA repression ( $P_{CMV}$ \_TO\_NanoDeg\_IRES\_EKRAB). The circuit components were integrated into the genome of HEK293 cells using lentiviral transduction, cells selected, and single clones expanded and transiently transfected for tTA expression. The monoclonal population displaying highest GFP fold change upon treatment with erythromycin (Em) ( $10 \,\mu g \, \text{ml}^{-1}$ ,  $24 \,\text{h}$ ) (Supplementary Fig. 5) was used as master cell line (HEK293-MCL).

The use of small-molecule-dependent transcription factors tTA and EKRAB enables tuning of the gene signal amplifier for monitoring target genes with different levels of basal expression through small-molecule dosage. Modulating the medium concentration of tetracycline (Tc) and Em controls the amount of active tTA and EKRAB in the system: optimal Tc and Em concentrations result in minimal GFP output under basal conditions and maximal change in GFP fluorescence upon induction of target gene expression.

To evaluate the gene signal amplifier platform, we integrated the IRES\_tTA cassette downstream of BIP in HEK293-MCL cells using CRISPR-Cas9 based on homologous direct-repair (generating the MCL/BIP-tTA cell line). We monitored the GFP fluorescence of MCL/BIP-tTA cells as a function of Tc and Em concentration under basal conditions (Fig. 2f and Supplementary Fig. 6) and upon treatment with tunicamycin (1 µg ml<sup>-1</sup>, 48 h) (Fig. 2g and Supplementary Fig. 6) using flow cytometry. MCL/ BIP-tTA cells cultured in media not supplemented with Em display a GFP fluorescence output comparable to that of the parental cell line HEK293-MCL (data not shown). We determined the Tc and Em concentrations (Tc, 50 ng ml<sup>-1</sup>; Em, 100 ng ml<sup>-1</sup>) that produce maximal signal amplification upon cell exposure to the stimulus (Fig. 2h). Notably, the MCL/BIP-tTA cell line generates a ~65-fold signal amplification upon tunicamycin treatment under the conditions of this study. Furthermore, the coefficient of variation on the GFP fold change values between independent experiments was below 15% (Supplementary Fig. 7a), underscoring the robustness of the gene signal amplifier compared with reported methods for monitoring BIP expression32.

The gene signal amplifier resolves gene dynamics. To characterize the *BIP* reporter, we knockdown *BIP* using short hairpin RNA (shRNA). MCL/BIP-tTA cells were transfected with a plasmid expressing a *BIP*-specific shRNA sequence (shBIP), treated with tunicamycin (10 μg ml<sup>-1</sup>, 1 h) and analyzed 48 h post treatment by flow cytometry. Control MCL/BIP-tTA cells transfected with an empty plasmid or a plasmid expressing a nontargeting scrambled shRNA (shNTC) displayed ~25-fold change in GFP output upon tunicamycin treatment. MCL/BIP-tTA cells expressing shBIP displayed ~3-fold change in GFP output upon tunicamycin treatment under the same conditions (Supplementary Fig. 8), indicating that the fluorescent output of MCL/BIP-tTA cells depends on *BIP* expression.

To evaluate the gene signal amplification, we compared the gene signal amplifier (MCL/BIP-tTA) with the reporter based on direct chromosomal integration of *GFP* at the 3′ of the target gene (BIP-GFP). We found the GFP output of MCL/BIP-tTA cells to be ~10-fold lower than that of BIP-GFP cells under basal conditions, and ~3-fold higher than that of the BIP-GFP cells upon tunicamycin treatment (1  $\mu$ g ml<sup>-1</sup>, 48 h) (Fig. 3a–c). As a result, tunicamycin treatment conditions causing a ~1.8-fold change in the GFP output of BIP-GFP cells result in a ~65-fold change in the GFP output of MCL/BIP-tTA cells (Fig. 3d and Supplementary Fig. 9), pointing

to the role of transcriptional and post-translational control of GFP output in the amplification of the signal output. The bimodal distribution of MCL/BIP-tTA cells treated with tunicamycin (Fig. 3b) is likely to result from the intrinsic heterogeneity of genetically identical populations<sup>33</sup>. The transcriptional and post-translational processes mediating signal amplification in MCL/BIP-tTA cells result in a 12-h lag time (Supplementary Fig. 10).

To evaluate the sensitivity of the gene signal amplifier to changes in target gene expression, we monitored the response of MCL/BIP-tTA cells to short pulses of ER stress. MCL/BIP-tTA cells were exposed to tunicamycin (2.5, 5 and  $10\,\mu\mathrm{g\,ml^{-1}}$ ) for short time intervals (15, 30 and 60 min), and GFP fluorescence was measured 24 h post treatment. MCL/BIP-tTA cells produced distinct GFP outputs for the different duration of the treatment under the same tunicamycin concentration conditions, and for the different tunicamycin concentration under the same duration of treatment (Fig. 3e), indicating gradual amplification of GFP signal proportional to *BIP* upregulation.

To explore the dynamic resolution of the target gene expression achieved with the gene signal amplifier, we monitored the fluorescence of MCL/BIP-tTA cells induced with tunicamycin (10 µg ml<sup>-1</sup>, 1 h) and treated with Tc (10 µg ml<sup>-1</sup>) 36 h post induction. Addition of an excess of Tc is expected to block tTA-mediated activation of GFP expression: monitoring GFP fluorescence as a function of time allows evaluating GFP decay upon reduction of tTA in the system. The output signal of cells treated with Tc decayed to half of its maximum value after about 12 h and to the initial value after 36 h of treatment, while the output signal of cells not treated with Tc does not display significant change during the same time interval (Fig. 3f), indicating that the output of the gene signal amplifier reflects the dynamic behavior of the input.

To evaluate the contribution of the NanoDeg to the dynamic properties of the gene signal amplifier, we built a BIP reporter cell line lacking the NanoDeg (MCL/BIP-tTA ΔNanoDeg cells; Supplementary Fig. 11a). MCL/BIP-tTA ΔNanoDeg cells cultured in the presence of optimal Tc and Em concentrations (Tc, 100 ng ml<sup>-1</sup>; Em, 500 ng ml<sup>-1</sup>) (Supplementary Fig. 11b) were induced with tunicamycin (10 µg ml<sup>-1</sup>, 1 h) and treated with Tc (10 µg ml<sup>-1</sup>) 36 h post induction. The output signal of MCL/BIP-tTA ΔNanoDeg cells was unaltered after 12h of treatment with Tc (a treatment condition that resulted in the decay of GFP signal to half of its initial value in MCL/BIP-tTA cells) and was reduced to ~40% of initial value after 36h (which resulted in complete decay to initial values in MCL/ BIP-tTA cells) (Fig. 3g,h). These results demonstrate the key role of the NanoDeg in the design of the gene signal amplifier, particularly for enhancing the dynamic resolution of the input. The output signal of MCL/BIP-tTA ΔNanoDeg cells was found to be significantly higher than that of MCL/BIP-tTA cells under basal conditions (Fig. 3i), but comparable to that MCL/BIP-tTA cells upon tunicamycin induction (Fig. 3j), supporting the results obtained from the model-guided design of the gene signal amplifier (Fig. 2).

The gene signal amplifier adapts to target gene features. To test the gene signal amplifier platform for monitoring expression of different target genes, we generated reporters of eight UPR targets (ERdj4, PPP1R15A (GADD34), SREBF1, DDIT3 (CHOP), WARS, TRIB3, EIF4 and CANX (refs. 12,34)) by integrating the IRES\_tTA cassette into the chromosome of HEK293-MCL cells at the 3′ of each target gene. We found the signal dynamic range upon tunicamycin induction to depend on Tc and Em concentrations and the optimal Tc and Em concentrations to be gene-specific (Fig. 4a–h).

A comparison of the dynamic range of GFP output of reporters based on chromosomal integration of *GFP* and reporters containing the gene signal amplifier revealed that the gene signal amplifier causes a dramatic increase in GFP signal output associated with the target gene expression. BIP-GFP, ERdj4-GFP and EIF4-GFP

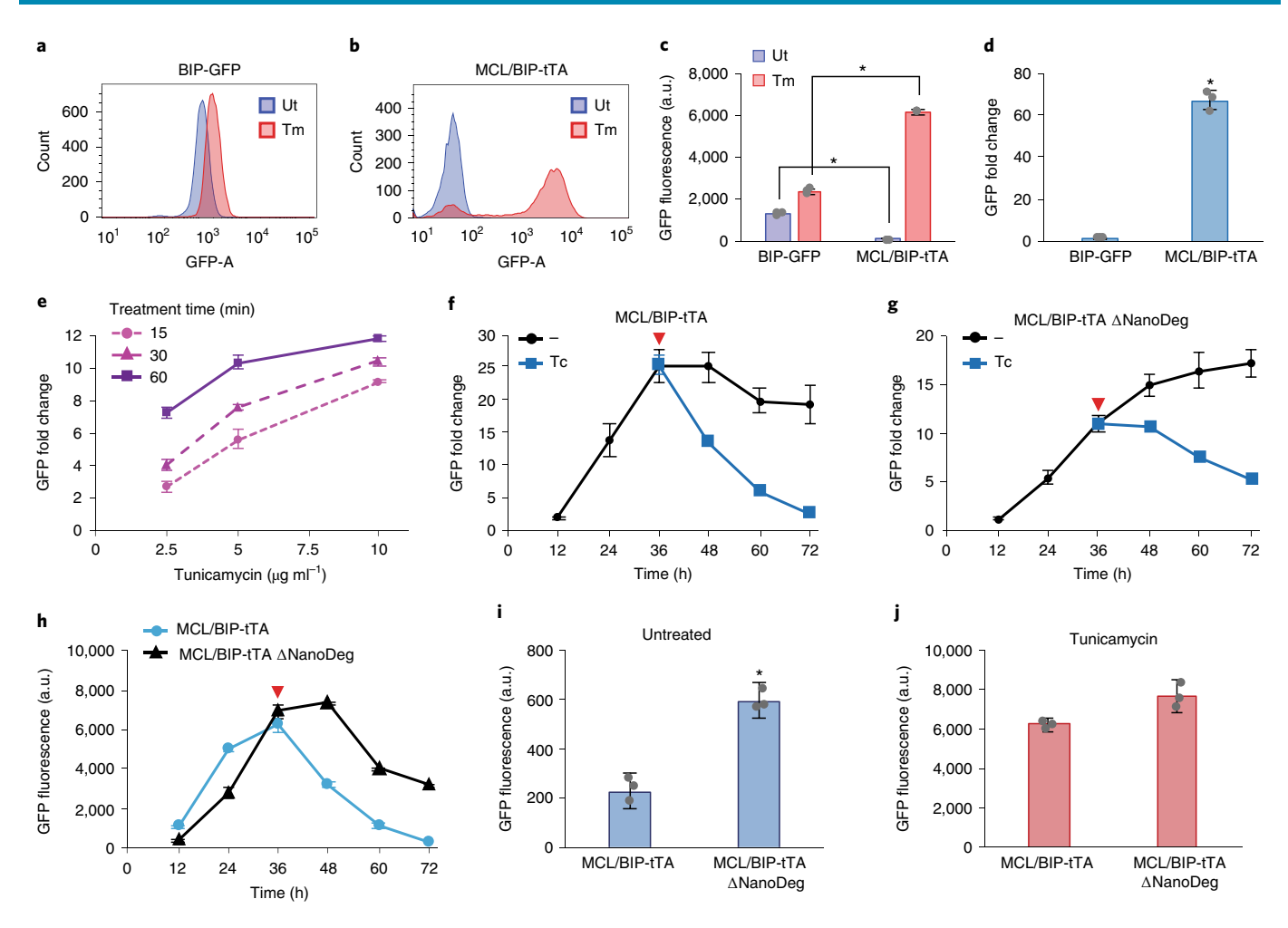


**Fig. 3 | Characterization of MCL/BIP-tTA cells. a,b**, Representative histograms of flow cytometry analyses of BIP-GFP cells (a) and MCL/BIP-tTA cells (b) untreated (blue) and treated with tunicamycin (1μg ml $^{-1}$ , 48 h; red). **c**, GFP fluorescence intensity of BIP-GFP and MCL/BIP-tTA cells treated as in **a** and **b**. Data are reported as mean ± s.d. (n = 3, \*P < 0.005). Ut, untreated; Tm, tunicamycin. **d**, GFP fold change of MCL/BIP-tTA and BIP-GFP cells obtained by normalizing the GFP fluorescence of cells treated with tunicamycin to that of untreated cells. Data are reported as mean ± s.d. (n = 3, \*P < 0.0005). **e**, Flow cytometry analyses of MCL/BIP-tTA cells treated with tunicamycin (2.5, 5 and 10 μg ml $^{-1}$ ) for different incubation times (15, 30 and 60 min) and measured 24 h post treatment. GFP fold change values were obtained by normalizing the GFP fluorescence values of cells treated with tunicamycin to that of untreated cells. Data are reported as mean ± s.d. (n = 3). **f**,**g**, Flow cytometry analyses of MCL/BIP-tTA (**f**) and MCL/BIP-tTA ΔNanoDeg (**g**) cells treated with tunicamycin (10 μg ml $^{-1}$ , 1h) and measured every 12 h post treatment. Tc (10 μg ml $^{-1}$ ) was added to the media 36 h post treatment (red triangle). MCL/BIP-tTA ΔNanoDeg cells were cultured in media supplemented with Tc (100 ng ml $^{-1}$ ) and Em (500 ng ml $^{-1}$ ). Data are reported as mean ± s.d. (n = 3). **i**, Flow cytometry analysis of MCL/BIP-tTA and MCL/BIP-tTA ΔNanoDeg cells were cultured in media supplemented with Tc (100 ng ml $^{-1}$ ) and Em (500 ng ml $^{-1}$ ). Data are reported as mean ± s.d. (n = 3). **i**, Flow cytometry analysis of MCL/BIP-tTA and MCL/BIP-tTA ΔNanoDeg reported as GFP fluorescence measurements under basal conditions (**i**) (untreated) and upon treatment with tunicamycin (**j**) (1 μg ml $^{-1}$ , 48 h). Data are reported as mean ± s.d. (n = 3, \*P < 0.005).

cells displayed 1.8-, 1.5- and 1.4-fold increase in GFP signal upon treatment with tunicamycin (1 µg ml $^{-1}$ , 48 h), whereas MCL/BIP-tTA, MCL/ERdj4-tTA and MCL/EIF4-tTA presented a 65-, 52- and 34-fold increase in GFP signal (Supplementary Fig. 12), indicating that the gene signal amplifier results in ~35-, ~34- and ~24-fold amplification of the output associated with BIP, ERdj4 and EIF4 expression, respectively, compared with direct chromosomal integration of GFP (Supplementary Fig. 12).

Because the expression of the target gene is linked to that of tTA, we explored the relationship between the target gene basal expression and the optimal Tc concentration. To evaluate the target gene basal expression, we measured the mRNA levels of the UPR target genes using RT-qPCR and the GFP signal of each cell line treated with an excess of Em  $(10\,\mu g\,ml^{-1})$  (Fig. 4i). We observed a correlation between the target gene basal expression

(Fig. 4i) and the Tc dose resulting in maximal dynamic range of GFP output (Fig. 4a-h). Reporters of genes presenting low basal expression (that is, *ERdj4*, *GADD34*, *SREBF1* and *CHOP*) displayed maximal change in GFP expression in the absence of Tc and a decrease in GFP fold change upon addition of Tc (Fig. 4a-d), consistent with the notion that uninduced conditions result in low levels of tTA, which are reduced to suboptimal concentrations upon addition of Tc. Reporters presenting high target gene basal expression, on the other hand, required addition of Tc to generate maximal increase in GFP output upon UPR induction (Fig. 4e-h). Moreover, the optimal Tc concentration increased with increase in the target gene basal expression, indicating that inactivation of the pool of tTA due to the target gene basal expression results in lowered basal GFP signal in the absence of tunicamycin and maximal fold change in GFP signal upon tunicamycin treatment.

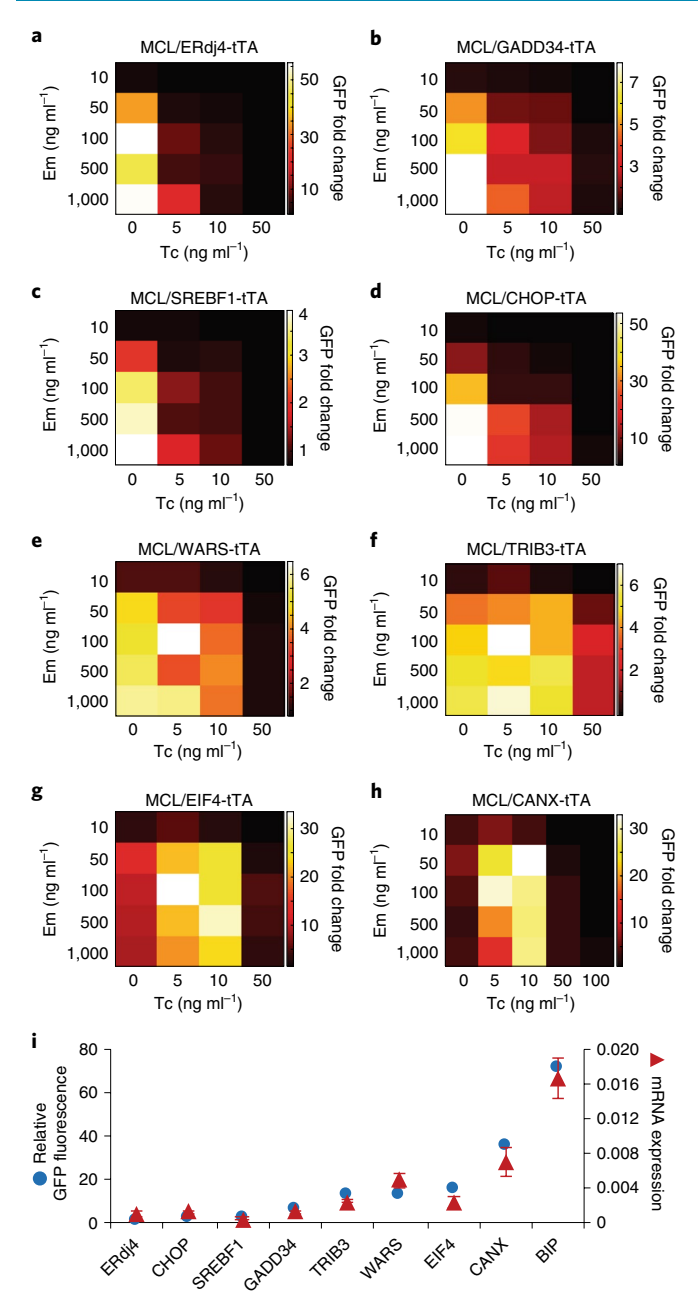


**Fig. 4 | Characterization of the multiplex UPR reporter system. a-h,** GFP output MCL/ERdj4-tTA (**a**), MCL/GADD34-tTA (**b**), MCL/SREBF1-tTA (**c**), MCL/CHOP-tTA (**d**), MCL/WARS-tTA (**e**), MCL/TRIB3-tTA (**f**), MCL/ EIF4-tTA (**g**) and MCL/CANX-tTA (**h**) cells as a function of Tc and Em concentration. GFP fold change values were obtained by normalizing the GFP fluorescence values of cells treated with tunicamycin (1 μg ml<sup>-1</sup>, 48 h) to that of untreated cells. Data are reported as mean (n = 3). (**i**) Relative GFP fluorescence output (blue circles) and mRNA expression levels (red triangles) of ERDj4, CHOP, SREBF1, GADD34, TRIB3, WARS, EIF4, CANX and BIP of cells from **a-h** under uninduced conditions. Relative GFP fluorescence values were obtained by normalizing the GFP fluorescence values of each reporter cell line to that of the parental HEK293-MCL cells, treated with Em (10 μg ml<sup>-1</sup>). mRNA expression values were generated by normalizing the Ct values of the target genes to that of RNA18SN1 (18S RNA) and ACTB (Actin) genes, measured using RT-qPCR. Data are reported as mean  $\pm$  s.d. (n = 3).

Dosing Em tunes the sensitivity of the circuit to changes in tTA expression by adjusting the concentration of active EKRAB that controls expression of GFP output.

These results suggest that the gene signal amplifier can be potentially adapted for monitoring any target gene via chromosomal integration of the main regulator at the appropriate locus and dosage of the inducer Tc and Em.

A computational tool to model the gene signal amplifier. To generate a computational tool for predicting experimental conditions to monitor any target gene, we refined the mathematical model to account for intrinsic expression features of the target gene. The model parameters were fit to the measurements of GFP fluorescence from the comprehensive dataset of reporter cell lines by adjusting the gene-specific parameters, namely the rate of synthesis of the target gene under basal conditions ( $\beta_0$ ) and the fold change of expression of the target gene  $(f_c)$ , and keeping all other parameters constant (Supplementary Note). Simulation of the GFP output (Supplementary Fig. 13) revealed that the model generates an accurate prediction of the GFP output (average coefficient of determination  $R^2 = 0.9$ ; Supplementary Fig. 14). The estimated basal rates of synthesis ( $\beta_0$ ) of the UPR target genes were proportional to the basal fluorescence of the corresponding reporter cell lines (Fig. 5a and Supplementary Fig. 15a), and the estimated fold changes of expression  $(f_c)$  were proportional to the change in fluorescence upon UPR induction (Fig. 5b and Supplementary Fig. 15b).

We next analyzed the effect of the gene-specific parameters (that is, the basal rate of synthesis ( $\beta_o$ ) and the fold change of expression ( $f_c$ )) on the optimal Tc and Em concentrations, which were predicted by simulating GFP expression as a function of basal rate of synthesis and fold change of expression (Fig. 5c,d). The optimal Tc concentration was found to increase as a function of both gene-specific parameters, confirming that tTA activity reflects the expression features of the target gene (Fig. 5c), while the optimal Em concentration depended mainly on the target gene fold change of expression (Fig. 5d), supporting the notion that EKRAB activity can be modulated to tune the gene signal amplifier to changes in tTA expression.

To test whether the model generates an accurate prediction of the conditions resulting in maximal signal amplification, we estimated the optimal Tc and Em concentrations based on the estimated basal rate of synthesis and fold change of expression of the target gene. The predicted optimal Tc and Em concentrations of MCL/SREBF1-tTA, MCL/GADD34-tTA, MCL/ERdj4-tTA and MCL/CHOP-tTA were identical to those determined experimentally. A comparison of the GFP fold change of MCL/WARS-tTA, MCL/TRIB3-tTA, MCL/EIF4-tTA, MCL/CANX-tTA and MCL/BIP-tTA cells experimentally treated with the model-predicted optimal Tc and Em doses and with optimal Tc and Em doses determined from the limited subset of conditions experimentally tested (Fig. 4a–h) revealed that the signal amplification produced by model-predicted Tc and Em concentrations is at least as high as that obtained using concentrations determined experimentally or improved dramatically (Fig. 5e–i).

To validate the use of the mathematical model, we investigated the expression of the UPR target HERPUD1 (HERP) (ref. 12). An HEK293 HERP reporter cell line (MCL/HERP-tTA) was generated and characterized using the same subset of representative Tc and Em concentrations used in previous analyses to determine optimal Tc and Em doses experimentally (Supplementary Fig. 16). The basal rate of HERP synthesis  $(\beta_0)$  was obtained from measurements of the GFP signal of MCL/HERP-tTA cells cultured in the presence of an excess of Em (10 µg ml-1) under basal conditions and using the correlation between the estimated rate of synthesis and the GFP output of the set of UPR reporters (Fig. 5a). The fold change of HERP expression (f<sub>c</sub>) was obtained from the measurement of GFP output in the presence of tunicamycin using the model. The optimal Tc and Em concentrations were then predicted based on HERP-specific values of basal rate of synthesis and fold change of expression. Treatment of MCL/HERP-tTA cells with tunicamycin (1 μg ml<sup>-1</sup>, 48 h) in the presence of the model-predicted optimal Tc

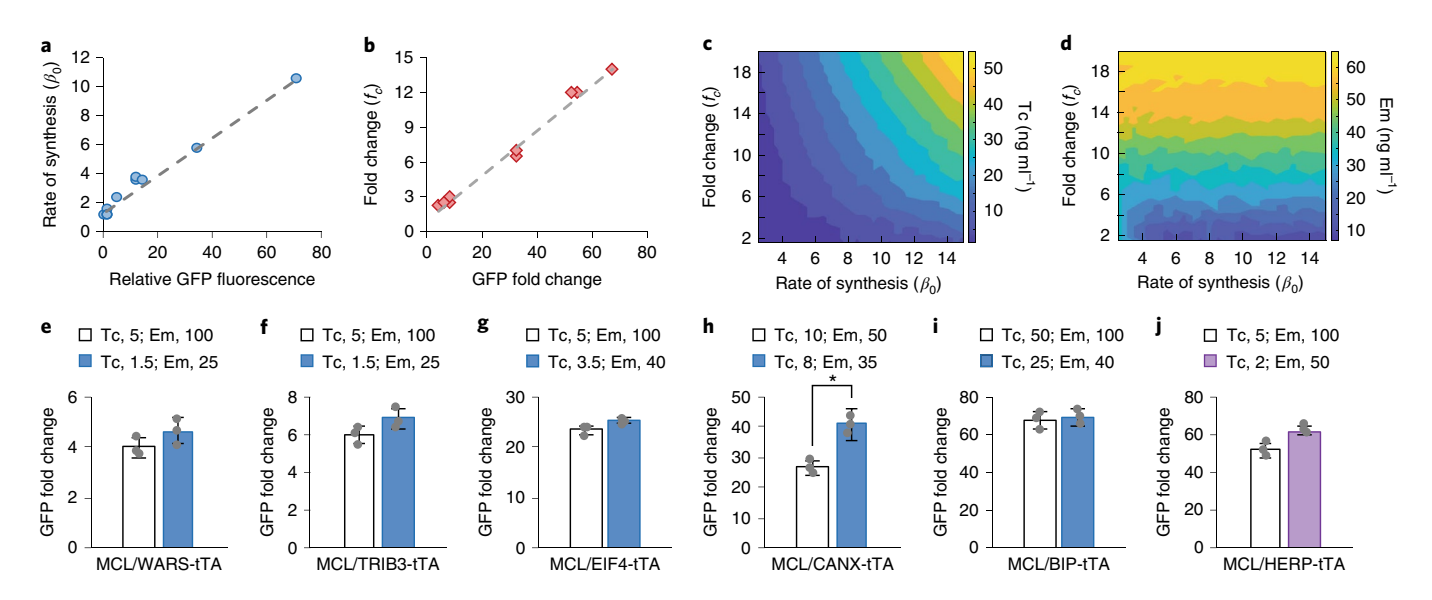


Fig. 5 | Development of a predictive model to adapt the gene signal amplifier for the detection of any cellular target. a, Correlation between the relative GFP fluorescence output of the reporter cell lines (that is, MCL/SREBF1-tTA, MCL/ERdj4-tTA, MCL/GADD34-tTA, MCL/CHOP-tTA, MCL/WARS-tTA, MCL/SREBF1-tTA, MCL/ERdj4-tTA, MCL/GADD34-tTA, MCL/CHOP-tTA, MCL/WARS-tTA, MCL/SREBF1-tTA, TRIB3-tTA, MCL/EIF4-tTA, MCL/CANX-tTA and MCL/BIP-tTA) and the estimated rate of synthesis of the respective target genes (that is, ERDj4, CHOP, SREBF1, GADD34, TRIB3, WARS, EIF4, CANX and BIP). Relative GFP fluorescence values were obtained by normalizing the GFP fluorescence values of each cell line to that of the parental HEK293-MCL cells, treated with Em (10 µg ml<sup>-1</sup>). GFP fluorescence values were measured using flow cytometry. Rate of synthesis values were obtained fitting the model to the experimental data. The gray dotted line represents the linear trendline of the data. b, Correlation between the measured maximum GFP fold change of the reporter cell lines as in a and the estimated fold change of the respective target genes. GFP fold change values were obtained by normalizing the GFP fluorescence values of cells treated with tunicamycin (1µg ml<sup>-1</sup>, 48 h) to that of untreated cells, quantified using flow cytometry. Fold change of the target genes were obtained fitting the model to the experimental data. The gray dotted line represents the linear trendline of the data. **c,d**, Optimal concentration of Tc (**c**) and Em (**d**) as a function of the rate of synthesis and the fold change of the target gene obtained using the mathematical model. e-i, Flow cytometry analyses of MCL/WARS-tTA (e), MCL/TRIB3-tTA (f), MCL/EIF4-tTA (g), MCL/CANX-tTA (h) and MCL/BIP-tTA (i) cells cultured in media supplemented with optimal Tc (ng ml<sup>-1</sup>) and Em (ng ml<sup>-1</sup>) experimentally determined (white bar) or model predicted (blue bar). GFP fold change values were obtained by normalizing the GFP fluorescence values of cells treated with tunicamycin (1µg ml<sup>-1</sup>, 48 h) to that of untreated cells. Data are reported as mean  $\pm$  s.d. (n=3, \*P<0.005). j, Flow cytometry analyses of MCL/HERP-tTA cells using optimal Tc and Em concentrations experimentally determined (Tc, 5 ng ml<sup>-1</sup>; Em, 100 ng ml<sup>-1</sup>; white bar) or model predicted (Tc, 2 ng ml<sup>-1</sup>; Em, 50 ng ml<sup>-1</sup>; purple bar). GFP fold change values were obtained by normalizing the GFP fluorescence values of cells treated with tunicamycin ( $1\mu g ml^{-1}$ , 48 h) to that of untreated cells. Data are reported as mean  $\pm$  s.d. (n=3).

and Em concentrations resulted in  $\sim$ 60-fold increase in GFP signal, which is as high as that obtained from testing the limited subset of Em and Tc concentrations (Fig. 5j). These results validate the use of the model as an integral part of the gene signal amplifier platform.

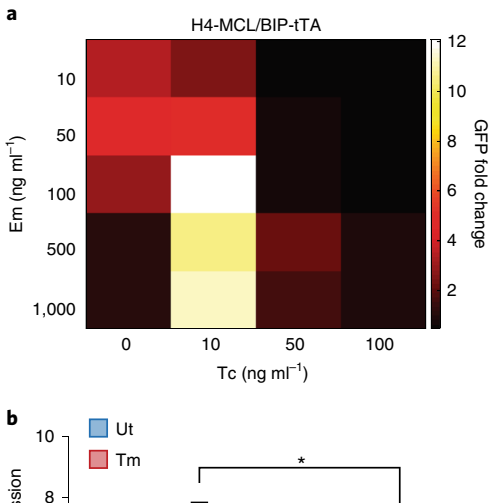
The gene signal amplifier adapts to distinct cellular contexts. To test whether the gene signal amplifier technology could be translated to other cell types, we created a *BIP* reporter using H4 neuroglioma cells<sup>35</sup>, which are often used to study the role of the UPR in the cellular pathogenesis of neurodegenerative diseases<sup>36</sup>. An H4 reporter of *BIP* expression was generated as described for HEK293 cells (H4-MCL/BIP-tTA). UPR induction using tunicamycin (1 μg ml<sup>-1</sup>, 48 h) resulted in ~12-fold increase in the GFP output of H4-MCL/BIP-tTA cells in the presence of optimal Tc (10 ng ml<sup>-1</sup>) and Em (100 ng ml<sup>-1</sup>) concentrations, supporting the use of the gene signal amplifier in H4 neuroglioma cells (Fig. 6a).

To compare the *BIP* reporters based on HEK293 and H4 cells, we measured *BIP* mRNA levels in HEK293 and H4 cells upon treatment with tunicamycin  $(1 \mu g \, \text{ml}^{-1}, 12 \, \text{h})$  (Fig. 6b). We observed a ~7- and ~4-fold increase in *BIP* expression in HEK293 and H4 cells, respectively, upon treatment with tunicamycin, reflecting the measured GFP outputs of the HEK293- and H4-based gene signal amplifier corresponding to a ~65- and ~12-fold increase in GFP signal, respectively.

#### Discussion

Our study establishes a method for monitoring gene expression with high sensitivity. The gene signal amplifier reported in

this study was envisioned as a two-module system composed of (1) a main regulator consisting of a tunable transcription factor that encodes information about regulation of the target gene expression, and (2) a circuitry that links the main regulator to a detectable reporter output and that is specially designed to amplify the output signal providing sensitive detection of the target gene dynamics. The main regulator (tTA) is linked to the target gene using an IRES from the encephalomyocarditis virus, which provides a well-characterized, scarless method to achieve gene co-expression. IRES variants producing different and precisely controlled ratios of expression between the co-expressed genes<sup>37</sup> could be explored to adjust the expression of the master regulator relative to the target gene, potentially tuning the sensitivity of the system. Previous studies have shown integration of transcriptional amplifiers and post-translational regulation to amplify output signals<sup>38-40</sup>. The circuitry topology reported herein links both transcriptional and post-translational control of the reporter to the activity of the main regulator. Transcriptional control is achieved here using EKRAB and can be adapted to other expression systems using a range of orthogonal, small-molecule-dependent transcriptional regulators<sup>30,41,42</sup>. Post-translational control is provided by the NanoDeg, which is responsible for the superior dynamic range of the gene signal amplifier platform. Notably, the NanoDeg is based on a fully customizable technology that could be adapted to target a seemingly unlimited number of protein structures<sup>31,43-45</sup> and through different modes and rates of degradations<sup>31</sup>, thus providing an additional layer of control to finely tune the performance of this gene signal amplifier platform.



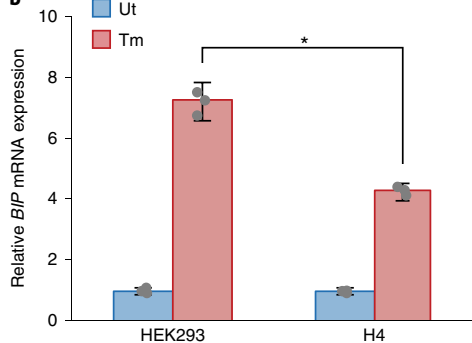


Fig. 6 | Translation of the gene signal amplifier to H4 neuroglioma cells.

**a**, Flow cytometry analyses of H4-MCL/BIP-tTA cells as a function of Tc and Em concentrations. GFP fold change values were obtained by normalizing the GFP fluorescence values of cells treated with tunicamycin ( $1\mu g \, ml^{-1}$ , 48 h) to that of untreated cells. **b**, BIP mRNA levels in HEK293 and H4 cells. Relative BIP expression values were obtained by normalizing BIP levels of cells treated with tunicamycin ( $1\mu g \, ml^{-1}$ , 12 h) to that of untreated cells, measured using RT-qPCR. Data are reported as mean  $\pm$  s.d. (n = 3,  $^*P$  < 0.005).

We validated the use of the gene signal amplifier by generating a multiplex reporter system to monitor markers of the UPR, a conserved stress-response signaling mechanism consisting of three integrated signaling pathways whose relative kinetics of activation are thought to determine cell fate<sup>11</sup>. We demonstrated that this platform technology can be used to monitor UPR target genes with different levels of basal expression and extent of induction by tuning the concentration of small molecules that function as inducers of the main regulator and circuitry components (Tc and Em).

The gene signal amplifier generates an output signal with superior sensitivity and dynamic resolution of the input compared with an analogous reporter system consisting of direct chromosomal integration of GFP linked to the target gene through the same IRES. The two-module system combines the advantage of chromosomal integration of the reporter enabling accurate detection of the target gene regulation with the powerful design of an orthogonal genetic network providing sensitive and facile detection of an output signal.

The mathematical model generated as part of this study allows customizing the gene signal amplifier platform to monitor any target gene and predicting optimal doses of small-molecule inducers, provided there is a derivative cell line with chromosomal integration of the main regulator at the 3′ of the target gene and a measurement of the target gene basal expression.

Adapting the platform technology developed as part of the present study to detection of gene expression requires generation of a master cell line in the relevant cell line. Subsequent chromosomal integration of the main regulator allows generating derivative genespecific reporter cell lines that can be built in parallel to obtain a

multiplex reporter system to monitor a comprehensive collection of marker genes. Generation of a BIP reporter based on H4 neuroglioma cells demonstrates that the gene signal amplifier can be transferred to other cell types. Notably, the extent of amplification of GFP output generated using the gene signal amplifier depends not only on the copy number of each circuit component integrated in the master cell line, but also on the activity of the promoters controlling the circuit components, which are known to vary depending on the cellular context<sup>46</sup>. Additional derivative gene-specific cell lines based on the H4 master cell line are needed to estimate the cell-line-specific parameters (that is, GFP synthesis rate ( $\beta_{GFP}$ ); rate of synthesis of the NanoDeg ( $\beta_{ND}$ ); tTA activation factor ( $f_{N_{TA}}$ ); EKRAB repression factor  $(f_{R_{EK}})$ ) and gene-specific parameters (that is, rate of synthesis of the target gene under basal conditions ( $\beta_0$ ) and the fold change of expression of the target gene  $(f_c)$ ). Such parameters will allow using the mathematical model to predict not only the optimal Tc and Em concentrations but also the fold change of expression  $(f_c)$  of the target genes across cellular contexts.

The gene signal amplifier system developed in this study provides a particularly appealing framework for conducting genetic and chemical screens<sup>47–49</sup> as it allows recapitulating the complexity of regulatory mechanisms controlling gene expression<sup>50</sup> and avoids the potential artifactual results that typically plague screens based on synthetic reporter systems.

The predictive value of the mathematical model combined with the unique design features of the two-module system generate the framework for a sensor-effector circuit that could be used for a variety of applications aimed at linking the expression level of a gene of interest to the expression of an effector molecule, such as a therapeutic agent, with exquisite control. This gene signal amplifier platform could be leveraged not only to study gene expression but also to precisely regulate cellular fate, thus opening the way to the design of novel cell-based therapeutic and diagnostic modalities.

#### Online content

Any methods, additional references, Nature Research reporting summaries, source data, extended data, supplementary information, acknowledgements, peer review information; details of author contributions and competing interests; and statements of data and code availability are available at <a href="https://doi.org/10.1038/s41589-020-0497-x">https://doi.org/10.1038/s41589-020-0497-x</a>.

Received: 13 August 2019; Accepted: 7 February 2020; Published online: 9 March 2020

#### References

- Hotamisligil, G. S. & Davis, R. J. Cell signaling and stress responses. Cold Spring Harb. Perspect. Biol. 8, a006072 (2016).
- Hetz, C. & Saxena, S. ER stress and the unfolded protein response in neurodegeneration. Nat. Rev. Neurol. 13, 477–491 (2017).
- Volpe, C. M. O., Villar-Delfino, P. H., Dos Anjos, P. M. F. & Nogueira-Machado, J. A. Cellular death, reactive oxygen species (ROS) and diabetic complications. *Cell Death Dis.* 9, 119 (2018).
- Buono, R. & Longo, V. D. Starvation, stress resistance, and cancer. Trends Endocrinol. Metab. 29, 271–280 (2018).
- Tahmasebi, S., Khoutorsky, A., Mathews, M. B. & Sonenberg, N. Translation deregulation in human disease. *Nat. Rev. Mol. Cell Biol.* 19, 791–807 (2018)
- Butte, A. The use and analysis of microarray data. Nat. Rev. Drug Discov. 1, 951–960 (2002).
- Nolan, T., Hands, R. E. & Bustin, S. A. Quantification of mRNA using real-time RT-PCR. Nat. Protoc. 1, 1559–1582 (2006).
- Draghici, S., Khatri, P., Eklund, A. C. & Szallasi, Z. Reliability and reproducibility issues in DNA microarray measurements. *Trends Genet.* 22, 101–109 (2006).
- Catarino, R. R. & Stark, A. Assessing sufficiency and necessity of enhancer activities for gene expression and the mechanisms of transcription activation. *Genes Dev.* 32, 202–223 (2018).
- 10. Ran, F. A. et al. Genome engineering using the CRISPR–Cas9 system. Nat. Protoc. 8, 2281–2308 (2013).

- Hetz, C. The unfolded protein response: controlling cell fate decisions under ER stress and beyond. Nat. Rev. Mol. Cell Biol. 13, 89–102 (2012).
- 12. Shoulders, M. D. et al. Stress-independent activation of XBP1s and/or ATF6 reveals three functionally diverse ER proteostasis environments. *Cell Rep.* 3, 1279–1292 (2013).
- 13. Walter, F., Schmid, J., Düssmann, H., Concannon, C. G. & Prehn, J. H. M. Imaging of single cell responses to ER stress indicates that the relative dynamics of IRE1/XBP1 and PERK/ATF4 signalling rather than a switch between signalling branches determine cell survival. *Cell Death Differ.* 22, 1502–1516 (2015).
- Walter, P. & Ron, D. The unfolded protein response: from stress pathway to homeostatic regulation. Science 334, 1081–1086 (2011).
- 15. Haze, K., Yoshida, H., Yanagi, H., Yura, T. & Mori, K. Mammalian transcription factor ATF6 is synthesized as a transmembrane protein and activated by proteolysis in response to endoplasmic reticulum stress. *Mol. Biol. Cell* **10**, 3787–3799 (1999).
- Klemm, S. L., Shipony, Z. & Greenleaf, W. J. Chromatin accessibility and the regulatory epigenome. Nat. Rev. Genet. 20, 207–220 (2019).
- 17. Soutourina, J. Transcription regulation by the Mediator complex. *Nat. Rev. Mol. Cell Biol.* **19**, 262–274 (2018).
- Schoenfelder, S. & Fraser, P. Long-range enhancer-promoter contacts in gene expression control. Nat. Rev. Genet. 20, 437–455 (2019).
- Han, J. et al. ER-stress-induced transcriptional regulation increases protein synthesis leading to cell death. Nat. Cell Biol. 15, 481–490 (2013).
- Adachi, Y. et al. ATF6 is a transcription factor specializing in the regulation of quality control proteins in the endoplasmic reticulum. *Cell Struct. Funct.* 33, 75–89 (2008).
- Bochkov, Y. & Palmenberg, A. Translational efficiency of EMCV IRES in bicistronic vectors is dependent upon IRES sequence and gene location. *Biotechniques* 41, 283–292 (2006).
- Mizuguchi, H., Xu, Z., Ishii-Watabe, A., Uchida, E. & Hayakawa, T. IRES-dependent second gene expression is significantly lower than cap-dependent first gene expression in a bicistronic vector. *Mol. Ther.* 1, 376–382 (2000).
- Lee, A.-H., Iwakoshi, N. N. & Glimcher, L. H. XBP-1 regulates a subset of endoplasmic reticulum resident chaperone genes in the unfolded protein response. *Mol. Cell. Biol.* 23, 7448–7459 (2003).
- 24. Yoshida, H. et al. ATF6 activated by proteolysis binds in the presence of NF-Y (CBF) directly to the cis-acting element responsible for the mammalian unfolded protein response. *Mol. Cell. Biol.* 20, 6755–6767 (2000).
- Vattem, K. M. & Wek, R. C. Reinitiation involving upstream ORFs regulates ATF4 mRNA translation in mammalian cells. *Proc. Natl Acad. Sci. USA* 101, 11269–11274 (2004).
- Wang, Y. et al. Activation of ATF6 and an ATF6 DNA binding site by the endoplasmic reticulum stress response. J. Biol. Chem. 275, 27013–27020 (2000).
- Dricu, A., Carlberg, M., Wang, M. & Larsson, O. Inhibition of N-linked glycosylation using tunicamycin causes cell death in malignant cells: role of down-regulation of the insulin-like growth factor 1 receptor in induction of apoptosis. *Cancer Res.* 57, 543–548 (1997).
- Lytton, J., Westlin, M. & Hanley, M. R. Thapsigargin inhibits the sarcoplasmic or endoplasmic reticulum Ca-ATPase family of calcium pumps. *J. Biol. Chem.* 266, 17067–17071 (1991).
- Gossen, M. & Bujard, H. Tight control of gene expression in mammalian cells by tetracycline-responsive promoters. *Proc. Natl Acad. Sci. USA* 89, 5547–5551 (1992).
- Weber, W. et al. Macrolide-based transgene control in mammalian cells and mice. Nat. Biotechnol. 20, 901–907 (2002).

- Zhao, W., Pferdehirt, L. & Segatori, L. Quantitatively predictable control of cellular protein levels through proteasomal degradation. ACS Synth. Biol. 7, 540–552 (2018).
- Oslowski, C. M. & Urano, F. Measuring ER stress and the unfolded protein response using mammalian tissue culture system. *Methods Enzymol.* 490, 71–92 (2011).
- Raser, J. M. & O'Shea, E. K. Noise in gene expression: origins, consequences, and control. Science 309, 2010–2013 (2005).
- Adamson, B. et al. A multiplexed single-cell CRISPR screening platform enables systematic dissection of the unfolded protein response. *Cell* 167, 1867–1882.e21 (2016).
- Rong, J. et al. Cell-based high-throughput luciferase reporter gene assays for identifying and profiling chemical modulators of endoplasmic reticulum signaling protein, IRE1. J. Biomol. Screen. 20, 1232–1245 (2015).
- Lindholm, D., Wootz, H. & Korhonen, L. ER stress and neurodegenerative diseases. Cell Death Differ. 13, 385–392 (2006).
- Venkatesan, A. & Dasgupta, A. Novel fluorescence-based screen to identify small synthetic internal ribosome entry site elements. Mol. Cell. Biol. 21, 2826–2837 (2001).
- Fernandez-Rodriguez, J. & Voigt, C. A. Post-translational control of genetic circuits using Potyvirus proteases. *Nucleic Acids Res.* 44, 6493–6502 (2016).
- Wang, B., Barahona, M. & Buck, M. Engineering modular and tunable genetic amplifiers for scaling transcriptional signals in cascaded gene networks. *Nucleic Acids Res.* 42, 9484–9492 (2014).
- Wan, X. et al. Cascaded amplifying circuits enable ultrasensitive cellular sensors for toxic metals. Nat. Chem. Biol. 15, 540–548 (2019).
- 41. Hörner, M. & Weber, W. Molecular switches in animal cells. FEBS Lett. 586, 2084–2096 (2012).
- Younger, A. K. D. et al. Development of novel metabolite-responsive transcription factors via transposon-mediated protein fusion. *Protein Eng. Des. Sel.* 31, 55–63 (2018).
- Muyldermans, S. Nanobodies: natural single-domain antibodies. Annu. Rev. Biochem. 82, 775–797 (2013).
- 44. Virant, D. et al. A peptide tag-specific nanobody enables high-quality labeling for dSTORM imaging. *Nat. Commun.* **9**, 1–14 (2018).
- Jayanthi, B. E. K., Zhao, W. & Segatori, L. Input-dependent post-translational control of the reporter output enhances dynamic resolution of mammalian signaling systems. *Methods Enzymol.* 622, 1–27 (2019).
- Qin, J. Y. et al. Systematic comparison of constitutive promoters and the doxycycline-inducible promoter. PLoS ONE 5, 3–6 (2010).
- Panganiban, R. A. et al. Genome-wide CRISPR screen identifies suppressors of endoplasmic reticulum stress-induced apoptosis. *Proc. Natl Acad. Sci. USA* 116, 13384–13393 (2019).
- 48. Potting, C. et al. Genome-wide CRISPR screen for PARKIN regulators reveals transcriptional repression as a determinant of mitophagy. *Proc. Natl Acad. Sci. USA* **115**, E180–E189 (2017).
- Pusapati, G. V. et al. CRISPR screens uncover genes that regulate target cell sensitivity to the morphogen Sonic Hedgehog. *Dev. Cell* 44, 113–129.e8 (2018).
- Donati, G., Imbriano, C. & Mantovani, R. Dynamic recruitment of transcription factors and epigenetic changes on the ER stress response gene promoters. *Nucleic Acids Res.* 34, 3116–3127 (2006).

**Publisher's note** Springer Nature remains neutral with regard to jurisdictional claims in published maps and institutional affiliations.

 $\ensuremath{\mathbb{G}}$  The Author(s), under exclusive licence to Springer Nature America, Inc. 2020

#### Methods

**Plasmids.** Lentiviral vectors were generated and maintained in Stbl3 *Escherichia coli* competent cells (catalog no. C7373-03; Thermo Fisher Scientific). All other plasmids were generated and maintained in DH5 $\alpha$  *E. coli* competent cells (catalog no. 11319019; Thermo Fisher Scientific). The primers used in this study are listed in Supplementary Table 1.

Plasmids containing the hSpCas9 gene expressed under the CMV promoter and a single guide RNA (sgRNA) that targets the 3' end of the coding sequence of selected target genes (DNAJB9, EIF4EBP1, HSPA5, SREBF1, PPP1R15A, TRIB3, HERPUD1, WARS, DDIT3 and CANX) were constructed using LentiCRISPRv2 plasmid (Addgene plasmid no. 52961) and appropriate oligos (Supplementary Table 1) according to the manufacturer's protocol, generating gene-specific LentiCRISPRv2 plasmids.

The donor plasmids were generated by first amplifying two  $\sim$ 1-kb sequences at the 3′ of the coding region of the target genes and immediately downstream the stop codons of the target genes, which serve as the homologous regions flanking integration (Supplementary Table 1). The two  $\sim$ 1-kb target-specific sequences for genes DNAJB9, EIF4EBP1, HSPA5, SREBF1, PPP1R15A, TRIB3, HERPUD1, WARS, DDIT3 and CANX were amplified from HEK293 chromosomal DNA by PCR using KAPA HiFi HotStart DNA (catalog no. KK2502; Kapa Biosystems).

pBIP\_IRES\_GFP, pERdj4\_IRES\_GFP and pEIF4\_IRES\_GFP donor plasmids were built using primer extension PCR to clone the *IRES\_eGFP\_loxPNeo* cassette, amplified from Oct4\_ires\_eGFP(loxneo) (Addgene plasmid no. 21547) and the ~1-kb gene-specific homologous sequences, into pcDNA3.1 (catalog no. V79020; Thermo Fisher Scientific) using type IIS restriction enzymes.

pBIP\_IRES\_tTA, pERdj4\_IRES\_tTA and pEIF4\_IRES\_tTA donor plasmids were generated by cloning tTA, amplified from ptTA<sup>31</sup>, into pBIP\_IRES\_GFP, pERdj4\_IRES\_GFP and pEIF4\_IRES\_GFP using BamHI and NotI restriction sites, thus replacing eGFP.

To construct the donor plasmids for integrating the *IRES\_tTA\_loxPNeo* cassette downstream *SREBF1*, *PPP1R15A*, *TRIB3*, *HERPUD1*, *WARS*, *DDIT3* and *CANX* genes, we first built a backbone plasmid containing the *IRES\_tTA\_loxPNeo* cassette amplified from pBIP\_IRES\_tTA, the *ori\_AmpR* cassette amplified from pcDNA3.1, modified to eliminate the BsaI restriction enzyme within *AmpR*, and two filler pieces, linked using four BsaI restriction enzyme sites. The resulting plasmid template was digested using BsaI and ligated to the ~1-kb gene-specific sequences, generating the donor plasmids pSREBF1\_IRES\_tTA, pGADD34\_IRES\_tTA, pTRIB3\_IRES\_tTA, pHERP\_IRES\_tTA, pWARS\_IRES\_tTA, pCHOP\_IRES\_tTA and pCANX\_IRES\_tTA.

p7TO\_ETR\_GFP was generated from pLenti\_CMV\_GFP\_Blast plasmid (Addgene plasmid no. 17445). The *7TO* promoter, consisting of seven repeats of the 19-base-pair Tc operator sequence and the CMV minimal promoter, which was amplified from pTRE\_tTA<sup>51</sup>, was cloned into pLenti\_CMV\_GFP\_Blast using ClaI and XbaI restriction sites, generating the plasmid p7TO\_GFP. The 4-*ETR* operator, consisting of four repeats of the ETR operator<sup>30,52</sup>, was generated by oligo assembly PCR and cloned into p7TO\_GFP using XbaI and BamHI restriction enzyme sites.

pTO\_NanoDeg\_IRES\_EKRAB was constructed by cloning the gene encoding the GFP-specific, degron-tagged nanobody (VHH<sub>ODC</sub>), amplified from pVHH\_ODC<sup>31</sup>, the *IRES* sequence, amplified from Oct4\_ires\_eGFP(lox neo), and *EKRAB*<sup>30,52</sup>, generated by oligo assembly PCR, into pLenti\_CMV/TO\_eGFP\_Puro (Addgene plasmid no. 17481) using XbaI and BamHI restriction enzyme sites.

pLKO.1\_shBIP and pLKO.1\_shNTC were generated using pLKO.1\_TRC cloning vector (Addgene plasmid no. 10878) engineered to express an shRNA targeting *BIP* gene (shBIP) or an shNTC according to the manufacturer's protocol (Supplementary Table 1). The sequence used to target *BIP* gene (5'-GAGCGCATTGATACTAGAAAT-3') was obtained from the RNA Interference Platform (Broad Institute).

pCMV\_iRFP, pCMV\_eGFP and ptTA were generated as previously described  $^{31,51}$ . pCMV5\_Flag\_XBP1s, pCGN\_ATF6 (1–373) and pRK\_ATF4 were purchased from Addgene (no. 63680, no. 27173 and no. 26114, respectively).

piRFP\_IRES\_GFP plasmid was generated by cloning the iRFP sequence, amplified from pCMV\_iRFP, the IRES sequence, amplified from Oct4\_ires\_eGFP(lox neo), and eGFP sequence, amplified from pLenti\_CMV\_GFP\_Blast, into pcDNA3.1 using XbaI and BamHI restriction enzyme sites.

Cell culture and transfections. HEK293 cells (catalog no. CRL-1573; ATCC) and HEK293T cells (catalog no. CRL-3216; ATCC) were cultured in DMEM/high glucose (catalog no. SH30243.01; Hyclone), supplemented with 10% FBS (catalog no. 12306–500ML; Sigma-Aldrich) and 1% penicillin–streptomycin–glutamine (PSQ; catalog no. SV30082.01; Hyclone), and maintained at 37 °C and 5% CO $_2$ . Cells were passaged using PBS (catalog no. 17–516 F; Lonza) and trypsin (TrypLE Express; catalog no. 12605–036; GIBCO).

Transient transfections were conducted by seeding cells onto 12-well plates or  $100 \times 20$ -mm² tissue culture dishes. After 24h, upon reaching 70–80% confluency, cells were transfected with 500 ng of DNA per well using JetPrime (catalog no. 114–15; Polyplus transfection) according to the manufacturer's protocol. The medium was replaced with fresh medium 24h post transfection, and cells were analyzed 48h post transfection unless otherwise indicated.

**Lentivirus production and transductions.** Third-generation lentiviruses were generated by seeding HEK293T cells onto  $100\times20\text{-mm}^2$  tissue culture dishes at a density of  $1\times10^6$  cells per dish. Cells were transfected with pTO\_NanoDeg\_ IRES\_EKRAB and p7TO\_ETR\_GFP, and the packaging plasmids pMLg/PRRE (Addgene plasmid no. 12251), pRSV-Rev (Addgene plasmid no. 12253) and pMD2.g (Addgene plasmid no. 12259) in a 2:5:2.5:3 ratio, respectively. The total DNA transfected per  $100\times20\text{-mm}^2$  tissue culture dish was  $5\,\mu g$ , consisting of  $0.8\,\mu g$  of pTO\_NanoDeg\_IRES\_EKRAB or p7TO\_ETR\_GFP,  $2\,\mu g$  of pMLg/PRRE,  $1\,\mu g$  of pRSV-Rev and  $1.2\,\mu g$  of pMD2.g plasmids, respectively. The medium was replaced with fresh medium  $8\,h$  post transfection and the virus-containing medium was collected after  $48\,h$ . The virus was concentrated using a Lenti-X concentrator (catalog no. 631232; Clontech) according to the manufacturer's protocol.

Viruses were titrated using RT-qPCR<sup>53</sup>. Briefly, the viral RNA was extracted using Quick-RNA Viral kit (Cat. No. R1034; Zymo Research) and complementary DNA synthesized using qScript cDNA SuperMix (catalog no. 95048-100; Quantabio). cDNA samples were analyzed by RT-qPCR using PerfeCTa SYBR (catalog no. 95072-012; Quanta Biosciences) and primers targeting the viral components *LTR-gag* and *WPRE* (Supplementary Table 1).

Cell transduction was conducted by seeding HEK293 cells onto 12-well plates at a density of  $1\times10^5$  cells per well. After 24h, the medium was replaced with medium containing  $9\times10^{10}$  virus particles per ml and  $8\,\mu g\,ml^{-1}$  polybrene (catalog no. NC9840454; Fisher Scientific Company). The virus-containing medium was replaced with fresh medium 24h post transduction.

**Reagents.** Tunicamycin (catalog no. T7765-5MG; Sigma-Aldrich), thapsigargin (catalog no. T9033-1MG; Sigma-Aldrich) and Em (catalog no. E5389-5G, Sigma-Aldrich) were dissolved in DMSO (catalog no. 472301; Sigma-Aldrich) to prepare a  $10\,\mathrm{mg\,ml^{-1}}$  stock solution. Tc (catalog no. T7660-5G; Sigma-Aldrich) was dissolved in H<sub>2</sub>O to prepare a  $10\,\mathrm{mg\,ml^{-1}}$  stock solution. Untreated samples were cultured in media supplemented with the vehicle.

**Flow cytometry analyses.** Cell were analyzed with a FACSCanto II flow cytometer (BD Biosciences). GFP fluorescence intensity was detected using a 488-nm laser and 530/30-nm emission filter. iRFP fluorescence intensity was detected using a 635-nm laser and 780/60-nm emission filter. At least 10,000 cells were recorded in each sample for analysis (Supplementary Fig. 17).

Generation of stable cell lines. To generate the cell lines BIP-GFP, ERdj4-GFP and EIF4-GFP, HEK293 cells were seeded onto 12-well plates and transfected with a gene-specific LentiCRISPRv2 plasmid and a donor plasmid (pBIP\_IRES\_GFP, pERdj4\_IRES\_GFP or pEIF4\_IRES\_GFP) in a 1:2 ratio. Cells were transferred into  $100 \times 20$ -mm² tissue culture dishes 48 h post transfection and selected for 2 weeks using  $1 \, \text{mg} \, \text{ml}^{-1} \, \text{G418}$  (catalog no. 345812; EMD Millipore).

To generate the HEK293 master cell line (HEK293-MCL), HEK293 cells were seeded onto 12-well plates and transduced with pTO\_NanoDeg\_IRES\_EKRAB and p7TO\_ETR\_GFP. Cells were transferred into  $100\times20\text{-mm}^2$  tissue culture dishes 48 h post transduction and selected for 2 weeks using  $5\,\mu\mathrm{g\,m}^{1-1}$  blasticidin (catalog no. ant-bl-1; InvivoGen) and  $1\,\mu\mathrm{g\,m}^{1-1}$  puromycin (catalog no. ant-pr-1; InvivoGen). Selected cells were transfected with pCMV\_tTA and treated with  $10\,\mu\mathrm{g\,m}^{1-1}$  Em for 24 h. Cells were analyzed with a FACSAriaII (BD Biosciences) to sort the cells presenting the highest GFP fluorescence (top 10% of the cell population).

To screen monoclonal cell populations, sorted cells were seeded onto 96-well plates containing DMEM with 20% FBS at a density of 0.5 cells per well, expanded, transfected with pCMV\_tTA and treated with 10  $\mu g$  ml $^{-1}$  Em for 24h. Cells were analyzed by flow cytometry to select the monoclonal population with highest change in GFP fluorescence upon transient transfection of pCMV\_tTA and treatment with Em. The selected monoclonal population was used as master cell line (HEK293-MCL) to generate gene-specific reporter cell lines.

Reporter cell lines for monitoring selected target genes (*DNAJB9*, *EIF4EBP1*, *HSPA5*, *SREBF1*, *PPP1R15A*, *TRIB3*, *HERPUD1*, *WARS*, *DDIT3* and *CANX*) were generated by transfecting HEK293-MCL cells with a target gene-specific LentiCRISPRv2 plasmid and a donor plasmid (pBIP\_IRES\_tTA, pEIF4\_IRES\_tTA, pER6J4\_IRES\_tTA, pSREBF1\_IRES\_tTA, pGADD34\_IRES\_tTA, pTRIB3\_IRES\_tTA, pHERP\_IRES\_tTA, pWARS\_IRES\_tTA, pCHOP\_IRES\_tTA or pCANX\_IRES\_tTA) in a 1:2 ratio. Transfected cells were transferred into 100×20-mm² tissue culture dishes 48 h post transfection and selected for 2 weeks using 1 mg ml<sup>-1</sup> G418.

Control samples for assessing potential off-target integration were generated by transfecting HEK293 cells with a LentiCRISPRv2 plasmid encoding a scrambled sgRNA sequence and a donor plasmid (pBIP\_IRES\_GFP, pEIF4\_IRES\_GFP, pERdj4\_IRES\_GFP, pBIP\_IRES\_tTA, pEIF4\_IRES\_tTA, pERdj4\_IRES\_tTA, pSREBF1\_IRES\_tTA, pGADD34\_IRES\_tTA, pTRIB3\_IRES\_tTA, pHERP\_IRES\_tTA, pWARS\_IRES\_tTA, pCHOP\_IRES\_tTA or pCANX\_IRES\_tTA) in a 1:2 ratio. Lack of off-target integration was verified by culturing transfected cells in medium supplemented with G418 (1 mg ml<sup>-1</sup>) and monitoring cell death.

**Western blot analyses.** Cells were washed with cold PBS and lysed using the cOmplete lysis-M buffer containing a protease inhibitor cocktail (catalog no.

4719956001; Roche) for 30 min on ice, maintaining continuous agitation. Cells were then sonicated at a frequency of 20 kHz for 10 s and centrifuged for 10 min (14,000g and 4 °C). The supernatant was collected for western blot analyses. Protein concentrations were determined using the Bradford assay (catalog no. 23236; Thermo Fisher Scientific). Aliquots containing 30  $\mu g$  of proteins were separated by SDS-PAGE and analyzed by immunoblotting. Blots were probed using rabbit monoclonal  $\alpha$ -BIP (1:2,000; catalog no. 3177; Cell Signaling Technology), chicken polyclonal  $\alpha$ -GFP (1:2,000; Cat. No. AS-29779; AnaSpec), rabbit monoclonal  $\alpha$ -GAPDH (1:8,000; Cat. No. sc-47724; Santa Cruz Biotechnology) and appropriate horseradish peroxidase-conjugated secondary antibodies (m-IgGk BP-HRP, catalog no. sc-516102; m-IgG-HRP, catalog no. sc-2357; Santa Cruz Biotechnology). Blots were visualized using SuperSignal West Pico PLUS chemiluminescent substrate (catalog no. 34580; Thermo Fisher Scientific) and an ImageQuant LAS 4000 (GE Healthcare Life Science).

RT-qPCR. RNA was extracted using RNeasy Plus Mini kit (catalog no. 74134; Qiagen) and cDNA synthesized using qScript cDNA SuperMix (catalog no. 95048-100; Quanta Biosciences) following manufacturer's procedures. RT-qPCR reactions were performed using PerfecTa SYBR Green FastMix (catalog no. 95072-012; Quanta Biosciences) in a CFX96 Real-Time PCR Detection System (Bio-Rad) using appropriate primers (Supplementary Table 1).

Genomic PCR. Genomic DNA was extracted using E.Z.N.A Tissue DNA kit (catalog no. D3396-02; Omega Bio-tek) according to the manufacturer's protocol. PCR-mediated amplification of genomic DNA was performed using KAPA HiFi HotStart DNA and appropriate primers (Supplementary Table 1). The PCR products were resolved by electrophoresis on a 1% Tris-acetate-EDTA agarose gel, stained with ethidium bromide and visualized by UV light (Supplementary Fig. 18).

Confocal microscopy. Cells were seeded onto glass coverslips at a density of  $1\times 10^5$  cells per ml and treated with tunicamycin  $(10\,\mu\mathrm{g\,ml^{-1}},1\,h)$  24 h post seeding. Cells were washed with PBS 48 h post tunicamycin treatment and fixed with 4% paraformaldehyde (catalog no. AC416785000; Thermo Fisher Scientific). Nuclei were stained with Hoechst 33342 nuclear stain (catalog no. 62249; Thermo Fisher Scientific) and cells were washed with PBS. Coverslips were mounted onto glass slides and imaged using a Nikon A1 Confocal microscope (Nikon) and the NIS-Elements software (Nikon). The acquired images were processed using ImageJ software (National Institutes of Health).

**Statistical analysis.** Results of flow cytometry analyses are reported as mean  $\pm$  s.d. of three biological replicates. Fluorescence measurements from each replicate were obtained by calculating the median fluorescence of the population. Heatmap representations of data were created using MATLAB software (MathWorks) using the mean of three biological replicates. Statistical significance was calculated using a two-tailed Student's t-test and two-way analysis of variance.

**Mathematical model.** All details of mathematical models and computational methods are provided in the Supplementary Note. Simulations were performed with MATLAB (MathWorks).

**Reporting Summary.** Further information on research design is available in the Nature Research Reporting Summary linked to this article.

#### Data availability

The authors declare that data supporting the finding of this study are available within the article and its Supplementary Information. Additional data are available from the corresponding author upon reasonable request.

#### References

- Zhao, W., Bonem, M., McWhite, C., Silberg, J. J. & Segatori, L. Sensitive detection of proteasomal activation using the Deg-On mammalian synthetic gene circuit. *Nat. Commun.* 5, 3612 (2014).
- Kramer, B. P. et al. An engineered epigenetic transgene switch in mammalian cells. Nat. Biotechnol. 22, 867–870 (2004).
- Geraerts, M., Willems, S., Baekelandt, V., Debyser, Z. & Gijsbers, R. Comparison of lentiviral vector titration methods. BMC Biotechnol. 6, 34 (2006).

#### **Acknowledgements**

This work was funded by the National Science Foundation (grant no. MCB-1615562, grant no. CBET-1805317 and grant no. CBET-1930149) and the Welch Foundation (grant no. C-1824), and was conducted in part using resources of the Shared Equipment Authority at Rice University. This project was supported by the Cytometry and Cell Sorting Core at Baylor College of Medicine, with funding from the CPRIT Core Facility Support Award (grant no. CPRIT-RP180672), and by the NIH (grant no. P30 CA125123 and grant no. S10 RR024574).

#### **Author contributions**

C.A.O. and L.S. conceived the projected. C.A.O., B.B. and S.D.P. performed the experiments and C.A.O. and B.B. analyzed the data. C.A.O. and A.L.Y. generated the mathematical model. C.A.O. and L.S. wrote the manuscript.

#### **Competing interests**

The authors declare no competing interests.

#### Additional information

Supplementary information is available for this paper at https://doi.org/10.1038/s41589-020-0497-x.

Correspondence and requests for materials should be addressed to L.S.

Reprints and permissions information is available at www.nature.com/reprints.



Corresponding author(s):	Laura Segatori, Ph.D.
Last updated by author(s):	Aug 20, 2019

# **Reporting Summary**

X Life sciences

Behavioural & social sciences

Nature Research wishes to improve the reproducibility of the work that we publish. This form provides structure for consistency and transparency in reporting. For further information on Nature Research policies, see <u>Authors & Referees</u> and the <u>Editorial Policy Checklist</u>.

Statistics	
For all statistical analysis	es, confirm that the following items are present in the figure legend, table legend, main text, or Methods section.
n/a Confirmed	
☐ ☐ The exact sam	ple size $(n)$ for each experimental group/condition, given as a discrete number and unit of measurement
A statement o	n whether measurements were taken from distinct samples or whether the same sample was measured repeatedly
The statistical Only common to	test(s) used AND whether they are one- or two-sided ests should be described solely by name; describe more complex techniques in the Methods section.
A description	of all covariates tested
A description	of any assumptions or corrections, such as tests of normality and adjustment for multiple comparisons
A full description	ion of the statistical parameters including central tendency (e.g. means) or other basic estimates (e.g. regression coefficient) (e.g. standard deviation) or associated estimates of uncertainty (e.g. confidence intervals)
For null hypot  Give P values as	hesis testing, the test statistic (e.g. $F$ , $t$ , $r$ ) with confidence intervals, effect sizes, degrees of freedom and $P$ value noted exact values whenever suitable.
For Bayesian a	analysis, information on the choice of priors and Markov chain Monte Carlo settings
For hierarchic	al and complex designs, identification of the appropriate level for tests and full reporting of outcomes
Estimates of e	ffect sizes (e.g. Cohen's $d$ , Pearson's $r$ ), indicating how they were calculated
	Our web collection on <u>statistics for biologists</u> contains articles on many of the points above.
Software and c	ode
Policy information abou	ut <u>availability of computer code</u>
Data collection	BD FACSDiva Software (v8.0.1), FlowJo (v10.5.3), and ImageJ software (National Institutes of Health).
Data analysis	FlowJo (v10.5.3), Microsoft Excel 2016, and MATLAB 2019a (MathWorks)
	om algorithms or software that are central to the research but not yet described in published literature, software must be made available to editors/reviewers. deposition in a community repository (e.g. GitHub). See the Nature Research guidelines for submitting code & software for further information.
Data	
<ul><li>Accession codes, uni</li><li>A list of figures that l</li></ul>	ut <u>availability of data</u> nclude a <u>data availability statement</u> . This statement should provide the following information, where applicable: ique identifiers, or web links for publicly available datasets have associated raw data restrictions on data availability
	data supporting the finding of this study are available within the article and its Supplementary Information. Additional data are available author upon reasonable request.
<del></del>	fic reporting  elow that is the best fit for your research. If you are not sure, read the appropriate sections before making your selection.
	The second secon

Ecological, evolutionary & environmental sciences

# Life sciences study design

Sample size	No statistical method was used to predetermine sample size.
Data exclusions	No data were excluded.
Replication	All attempts at replication were successful, and we have indicated in each figure legend how many times each experiment was independently repeated.
Randomization	Randomization of samples in groups is not relevant to this study as no animal or clinical work was performed.
Blinding	Blinding experiments were not necessary as experimenters operated according to standard methods, conducted comprehensive analyses of all data, and obtained scientific conclusions. There was no personal preference for the experimental subjects and results.

# Reporting for specific materials, systems and methods

We require information from authors about some types of materials, experimental systems and methods used in many studies. Here, indicate whether each material, system or method listed is relevant to your study. If you are not sure if a list item applies to your research, read the appropriate section before selecting a response.

Materials & experimental systems	Methods
n/a Involved in the study	n/a Involved in the study
Antibodies	ChIP-seq
Eukaryotic cell lines	Flow cytometry
Palaeontology	MRI-based neuroimaging
Animals and other organisms	'
Human research participants	
Clinical data	
Antibodies	
synthetic peptide corres Anti-GFP Tag (AS-29779 GAPDH Antibody (0411) recombinant GAPDH of m-lgGk BP-HRP: sc-5161 Horseradish Peroxidase	#3177, Lot #9 Ref #09/2018, Cell Signaling Technology, rabbit monoclonal antibody produce against a sponding to residues surrounding Gly584 of human BiP, 1:2000 dilution.  1), Lot# RJ1901, AnaSpec EGT Group, rabbit polyclonal antibody 1:2000 dilution.  2): sc-47724, Lot# D0612, Santa Cruz Biotechnology, mouse monoclonal antibody raised against human origin, 1:1000 dilution.  102, Lot# D2518, Santa Cruz Biotechnology, mouse IgG kappa binding protein (m-IgGκ BP) conjugated to (HRP), 1:10000 dilution.  1RP: sc-2357, Lot# E1618, Santa Cruz Biotechnology, 1:10000 dilution.
Validation Antibodies used for Wes	stern Blot and validated by manufacturer.

## Eukaryotic cell lines

Policy information about cell lines

Cell line source(s)	HEK293 and HEK293T cells were purchased from ATCC. BIP-GFP, ERdj4-GFP, EIF4-GFP, HEK293-MCL, MCL/BIP-tTA, MCL/BIP-tTA dNanoDeg, MCL/ERdj4-tTA, MCL/GADD34-tTA, MCL/SREBF1-tTA, MCL/CHOP-tTA, MCL/WARS-tTA, MCL/TRIB3-tTA, MCL/EIF4-tTA, MCL/CANX-tTA, and MCL/HERP-tTA cells were generated in this study.
Authentication	HEK293 and HEK293T cells were purchased from ATCC and not further authenticated. HEK293 cells with genomic integration

generated in this study were confirmed by PCR and Western blot using standard protocols.

Mycoplasma contamination Cell lines were tested for mycoplasma contamination.

Commonly misidentified lines (See ICLAC register)

No commonly misidentified cell lines were used.

## Flow Cytometry

### Plots

Confirm that:	
The axis labels state the n	narker and fluorochrome used (e.g. CD4-FITC).
The axis scales are clearly	visible. Include numbers along axes only for bottom left plot of group (a 'group' is an analysis of identical markers).
All plots are contour plots	with outliers or pseudocolor plots.
A numerical value for nur	nber of cells or percentage (with statistics) is provided.
Methodology	
Sample preparation	Cells were trypsinized, collected on PBS and immediately transfered to ice.
Instrument	FACSCanto II flow cytometer (BD Biosciences)
Software	BD FACSDiva Software (v8.0.1) was used to interface with the flow cytometer and acquire sample data. Data was analyzed using Microsoft Excel 2016 and FlowJo (v10.5.3).
Cell population abundance	At least 10,000 cells were recorded in each sample for analysis. Sample acquisition was performed at $700 - 1,500$ event/s. All experiments are based on at least three independent biological replicates. Purity of cells was determined by forward versus side scatter gating.
Gating strategy	Cells were gated using linear forward scatter (FSC) area versus linear side scatter (SSC) area excluding the events at the bottom 20% of FSC-area and SSC-area values to eliminate cell debris and non-cell events, followed by gating on FSC-height versus FSC-

width and SSC-height versus SSC-width for aggregate exclusion. See Supplementary Figure 10.

 $\bowtie$  Tick this box to confirm that a figure exemplifying the gating strategy is provided in the Supplementary Information.